International Journal of Information, Control and Computer Sciences
ISSN: 2517-9942
Vol:10, No:1, 2016

Hyperspectral Imaging and Nonlinear Fukunaga-Koontz Transform Based Food Inspection

Hamidullah Binol, Abdullah Bal

***Abstract*—**Nowadays, food safety is a great public concern; therefore, robust and effective techniques are required for detecting the safety situation of goods. Hyperspectral Imaging (HSI) is an attractive material for researchers to inspect food quality and safety estimation such as meat quality assessment, automated poultry carcass inspection, quality evaluation of fish, bruise detection of apples, quality analysis and grading of citrus fruits, bruise detection of strawberry, visualization of sugar distribution of melons, measuring ripening of tomatoes, defect detection of pickling cucumber, and classification of wheat kernels. HSI can be used to concurrently collect large amounts of spatial and spectral data on the objects being observed. This technique yields with exceptional detection skills, which otherwise cannot be achieved with either imaging or spectroscopy alone. This paper presents a nonlinear technique based on kernel Fukunaga-Koontz transform (KFKT) for detection of fat content in ground meat using HSI. The KFKT which is the nonlinear version of FKT is one of the most effective techniques for solving problems involving two-pattern nature. The conventional FKT method has been improved with kernel machines for increasing the nonlinear discrimination ability and capturing higher order of statistics of data. The proposed approach in this paper aims to segment the fat content of the ground meat by regarding the fat as target class which is tried to be separated from the remaining classes (as clutter). We have applied the KFKT on visible and near-infrared (VNIR) hyperspectral images of ground meat to determine fat percentage. The experimental studies indicate that the proposed technique produces high detection performance for fat ratio in ground meat.

***Keywords*—**Food (Ground meat) inspection, Fukunaga-Koontz transform, hyperspectral imaging, kernel methods.

I. Introduction

HYPERSPECTRAL IMAGING (HSI) is an emerging technology that provides spatial and rich spectral information [1]. A hyperspectral image pixel can be represented by a vector that each component of the vector corresponds to a specific wavelength. For instance, the HYDICE (HYperspectral Digital Imagery Collection Experiment) hyperspectral sensor [2] has 210 spectral channels over the range 0.4-2.5 μm. This high-dimensional spectral information allows for the identification of materials based on their light absorption and reflection characteristics. The major hyperspectral applications include pixelwise classification which can be exploited for object recognition [3], target detection [4], land-cover/land use classification [5], biomedical applications [6], food inspection [7] etc.

Food-related problems are one of the high priority concerns of people's daily lives. That's why robust techniques for improving food safety and quality play a significant role. The scope of food safety comprises physical (e.g., texture, color), chemical (e.g., fat content, protein content, pH), and biological (e.g., bacterial counts) contamination. Estimation of quality and safety commonly contains classical visual inspection, in addition to chemical or biological determination analyses which are tiring, slow, and destructive [8]. As an alternative approach, HSI can produce both spatial and spectral information from the materials. More advantages are provided by these kinds of systems. As an illustration, such a system can simplify collecting spectral information in operator-defined regions, where corresponding relation between experimental spectra and reference values is guaranteed. HSI can also be utilized to create chemical maps to demonstrate distributions of features of interest. The benefits in spectroscopy and computer vision have yielded various applications in the food industry [7].

Fukunaga-Koontz transform (FKT) is one of the most efficient techniques for solving two-class problems. It is a favorite scheme method for quadratic correlation filters (QCF). The essence of QCF-based classification is to construct a coefficient matrix to make the two patterns discriminated in a margin as large as achievable.

The classical FKT has been developed with kernel machines for improving the capability of nonlinear discrimination. The nonlinear version of FKT, called as kernel FKT (KFKT), has been employed for target detection on infrared images [9], classification on hyperspectral images [10], and face recognition [11]. In this work, we suggested KFKT-based framework to determination of fat content in ground meat on hyperspectral images. The proposed framework focuses to separate the fat content of the ground meat visually by regarding the fat as target class. The KFKT-based technique tested on a VNIR hyperspectral image.

The rest of the paper is organized as follows. In Section II, brief information about hyperspectral data and employed classification method is provided. The experimental results present a performance analysis for suggested technique in Section III. Finally, concluding remarks are included in last section.

H. Binol is with the Department of Electronics and Communications Engineering, Yildiz Technical University, Istanbul 34220 Turkey (e-mail: hbinol@yildiz.edu.tr).

A. Bal is with the Department of Electronics and Communications Engineering, Yildiz Technical University, Istanbul 34220 Turkey, (corresponding author to provide phone: +90-212-383-5905; fax: +90-212-383-5882; e-mail: bal@yildiz.edu.tr).

This research was supported by the Scientific Research Projects Coordination Department of Yildiz Technical University under Project 2015-04-03-DOP03.

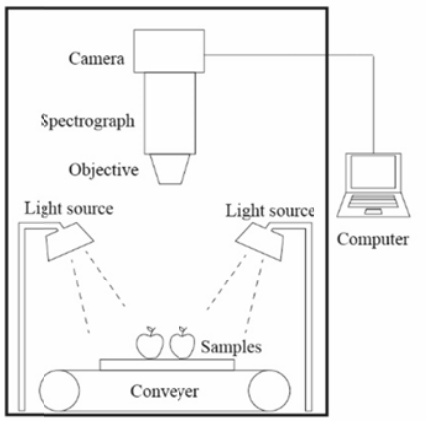

Fig. 1 Schematic diagram of a hyperspectral imaging system

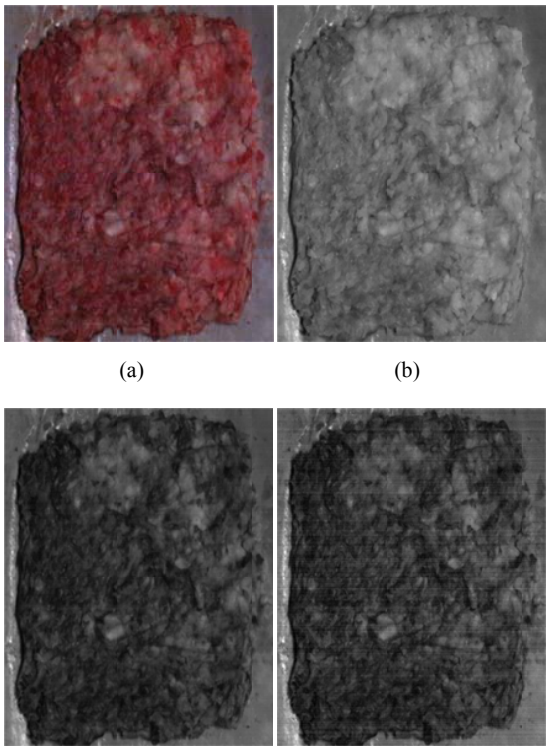

(a) (b)

(c) (d)

Fig. 2 Ground meat images: (a) RGB, (b) Wavelength is 460 nm, (c) Wavelength is 550 nm, and (d) Wavelength is 640 nm

II. Material and Methods

A. Image Acquisition and Correction

A typical laboratory hyperspectral imaging system consists of hardware and software. Its hardware platform contains common basic components, e.g., light source, spectrograph, objective lens, conveyer, and computer (see Fig. 1) [12]. The hyperspectral data set was gathered by the SPECIM sensor. It originally has 931 × 916 pixels and 196 spectral channels in the wavelength range of VNIR. After removing noisy bands, 187 bands were used in experiments. We worked a part of image which has 681 × 581 pixels. Fig. 2 shows RGB image and arbitrary three spectral channels of HSI data.

To obtain the reflectance spectrum, the spectral raw cube was corrected using two references, i.e., "white" and "black". The "white" is used to create the maximum reflectance conditions, which was acquired for a white ceramic tile under the same condition of the raw image; and a "black" one to characterize the no reflectance case, which was got by turning off the light source and entirely covering the lens with its dark beret. The corrected image was then computed by

$$I = \frac{I_0 - B}{W - B} \tag{1}$$

where I_0, W, and B represent the spectral raw image, white reference, and dark condition, respectively [13].

B. Classification Based on Nonlinear FKT

The FKT [14] is originally a feature selection and ordering approach. One feature extracted by FKT carries the meaningful information about one class; it has the least information about the other. Using this property, the coefficient matrix for QCF with FKT has been constructed in [15]. The main drawback of the FKT is that it considers second-order correlations, so it cannot capture the higher order statistical properties of data. That's why some researchers [9], [11], have extended the FKT to its nonlinear version via kernel machines. By operating a ϕ mapping scheme [16], the input data $\boldsymbol{x} \in \mathbb{R}^d$ is mapped into high-dimensional feature space called *Hilbert*, $\{\phi(\boldsymbol{x})\} \in \mathbb{F}$.

$$\phi: \begin{array}{c} \mathbb{R}^d \to \mathbb{F} \\ \boldsymbol{x} \to \phi(\boldsymbol{x}) \end{array} \tag{2}$$

Instead of knowing ϕ implicitly, the dot products in $\mathbb{F}$, i.e., $\langle \phi(\boldsymbol{x}_i), \phi(\boldsymbol{x}_j) \rangle$, can be evaluated using a positive definite function expressed by

$$K(\boldsymbol{x}_i, \boldsymbol{x}_j) = \langle \phi(\boldsymbol{x}_i), \phi(\boldsymbol{x}_j) \rangle \tag{3}$$

More details about kernel-based learning may be found in [17]. Experimentally, we utilized popular Gaussian Radial Basis Function (RBF) which has one free parameter. Some of the popular kernel functions are listed in Table I.

TABLE I
Common Used Kernel Functions

Kernels	Formula
RBF	$K(\boldsymbol{x}, \boldsymbol{y}) = exp(-\|\boldsymbol{x} - \boldsymbol{y}\|^2/2\sigma^2)$
Laplacian	$K(\boldsymbol{x}, \boldsymbol{y}) = exp(-\|\boldsymbol{x} - \boldsymbol{y}\|/\sigma)$
Linear	$K(\boldsymbol{x}, \boldsymbol{y}) = \boldsymbol{x}^{\mathrm{T}}\boldsymbol{y}$
Polynomial	$K(\boldsymbol{x}, \boldsymbol{y}) = (\boldsymbol{x}^{\mathrm{T}}\boldsymbol{y} + 1)^d$
Sigmoid	$K(\boldsymbol{x}, \boldsymbol{y}) = \tanh(v\boldsymbol{x}^{\mathrm{T}}\boldsymbol{y} + r)$

Considering training input vectors of two classes $\mathbf{C}_1 = [\boldsymbol{a}_1, \boldsymbol{a}_2, \ldots, \boldsymbol{a}_M]$ and $\mathbf{C}_2 = [\boldsymbol{b}_1, \boldsymbol{b}_2, \ldots, \boldsymbol{b}_N]$ which have been centered. Assume that $\mathbf{C}_1^{\phi}$ and $\mathbf{C}_2^{\phi}$ the mapped versions of input vectors belonging to class $\mathbf{C}_1$ and $\mathbf{C}_2$, respectively. Then,

corresponding covariance matrices defined as:

$$\begin{aligned}\mathbf{\Sigma}_1 &= \mathbf{C}_1^{\phi}\mathbf{C}_1^{\phi\,\mathrm{T}} \\ \mathbf{\Sigma}_2 &= \mathbf{C}_2^{\phi}\mathbf{C}_2^{\phi\,\mathrm{T}}\end{aligned} \tag{4}$$

where the superscript T represents the transpose operation. These matrices are called as kernel matrices and their elements can be computed via any kernel function represented in (3), i.e., $\mathbf{\Sigma}(i,j) = K(\boldsymbol{x}_i, \boldsymbol{x}_j)$. This phenomenon is dubbed as "kernel trick". $\mathbf{\Sigma}_1$ is constructed as:

$$\mathbf{\Sigma}_1 = \begin{bmatrix} K(\boldsymbol{a}_1,\boldsymbol{a}_1) & \cdots & K(\boldsymbol{a}_1,\boldsymbol{a}_M) \\ K(\boldsymbol{a}_2,\boldsymbol{a}_1) & \cdots & K(\boldsymbol{a}_2,\boldsymbol{a}_M) \\ \vdots & \ddots & \vdots \\ K(\boldsymbol{a}_M,\boldsymbol{a}_1) & \cdots & K(\boldsymbol{a}_M,\boldsymbol{a}_M) \end{bmatrix} \tag{5}$$

The eigenvalue/eigenvector decomposition of the sum of training kernel matrices is obtained by

$$\mathbf{\Sigma} = \mathbf{\Sigma}_1 + \mathbf{\Sigma}_2 = \mathbf{V}\mathbf{\Lambda}\mathbf{V}^{\mathrm{T}}. \tag{6}$$

The transform operator $\mathbf{P} = \mathbf{V}\mathbf{\Lambda}^{-1/2}$ is then designed and we can write following expression using (6)

$$\mathbf{P}^{\mathrm{T}}\mathbf{\Sigma}\mathbf{P} = \mathbf{I}. \tag{7}$$

$\mathbf{C}_1^{\phi}$ and $\mathbf{C}_2^{\phi}$ are transformed by operator $\mathbf{P}$. Thus, $\hat{\mathbf{C}}_1$ ($\hat{\mathbf{C}}_1 = \mathbf{P}^{\mathrm{T}}\mathbf{C}_1^{\phi}$) and $\hat{\mathbf{C}}_2$ ($\hat{\mathbf{C}}_2 = \mathbf{P}^{\mathrm{T}}\mathbf{C}_2^{\phi}$) are obtained. The transformed $\hat{\mathbf{C}}_1$ and $\hat{\mathbf{C}}_2$ constitute the following new covariance matrices:

$$\begin{aligned}\hat{\mathbf{\Sigma}}_1 &= \hat{\mathbf{C}}_1\hat{\mathbf{C}}_1^{\,\mathrm{T}} = \mathbf{P}^{\mathrm{T}}\mathbf{C}_1^{\phi}\mathbf{C}_1^{\phi\,\mathrm{T}}\mathbf{P} = \mathbf{P}^{\mathrm{T}}\mathbf{\Sigma}_1\mathbf{P} \\ \hat{\mathbf{\Sigma}}_2 &= \hat{\mathbf{C}}_2\hat{\mathbf{C}}_2^{\,\mathrm{T}} = \mathbf{P}^{\mathrm{T}}\mathbf{C}_2^{\phi}\mathbf{C}_2^{\phi\,\mathrm{T}}\mathbf{P} = \mathbf{P}^{\mathrm{T}}\mathbf{\Sigma}_2\mathbf{P}\end{aligned} \tag{8}$$

From (7) and (8), the key point of the KFKT can be easily derived that

$$\hat{\mathbf{\Sigma}} = \hat{\mathbf{\Sigma}}_1 + \hat{\mathbf{\Sigma}}_2 = \mathbf{P}^{\mathrm{T}}(\mathbf{\Sigma}_1 + \mathbf{\Sigma}_2)\mathbf{P} = \mathbf{I}. \tag{9}$$

If $\boldsymbol{v}$ is the eigenvector of $\hat{\mathbf{\Sigma}}_1$ corresponding to eigenvalue λ, then $(1-\lambda)$ must be the eigenvalue of $\hat{\mathbf{\Sigma}}_2$ corresponding to the same eigenvector. In other words, the most dominant eigenvectors in class one will be the incapable eigenvectors in class two [14]. Following formulas represent these deductions:

$$\begin{aligned}\hat{\mathbf{\Sigma}}_1\boldsymbol{v} &= \left(\mathbf{I} - \hat{\mathbf{\Sigma}}_2\right)\boldsymbol{v} = \lambda\boldsymbol{v} \\ \hat{\mathbf{\Sigma}}_2\boldsymbol{v} &= (\mathbf{I} - \lambda)\boldsymbol{v}\end{aligned} \tag{10}$$

To determine the class of test vector $\boldsymbol{z}$, the QCF approach is employed [14], [18]. If we can construct the optimal coefficient matrix, the output of its belonging to the test vector will be positive or larger for $\boldsymbol{z} \in \mathbf{C}_1$, and negative or smaller for $\boldsymbol{z} \in \mathbf{C}_2$. Matrix elements of $\mathbf{V}$, $\boldsymbol{v}_i\,(i = 1, \cdots, M)$, are eigenvectors corresponding to the eigenvalues of $\hat{\mathbf{\Sigma}}_1$ arranged in descending order as $\lambda_1 \geq \lambda_2 \geq \ldots \geq \lambda_M \geq 0$. The first m_1 eigenvectors ($\mathbf{V}_1$) represent the class one while the rest of the eigenvectors ($\mathbf{V}_2$) represent the class two:

$$\begin{aligned}\mathbf{V}_1 &= [\boldsymbol{v}_1, \boldsymbol{v}_2, \ldots, \boldsymbol{v}_{m_1}] \\ \mathbf{V}_2 &= [\boldsymbol{v}_M, \boldsymbol{v}_{M-1}, \ldots, \boldsymbol{v}_{M-m_2+1}]\end{aligned} \tag{11}$$

Output of the classification system can be found as:

$$\mathrm{y}_{\mathrm{out}} = \mathbf{R}_1^{\mathrm{T}}\mathbf{R}_1 - \mathbf{R}_2^{\mathrm{T}}\mathbf{R}_2 \tag{12}$$

where, $\mathbf{R}_1$ is $\mathbf{V}_1{}^{\mathrm{T}}\hat{\boldsymbol{z}}^{\phi}$, $\mathbf{R}_2$ is $\mathbf{V}_2{}^{\mathrm{T}}\hat{\boldsymbol{z}}^{\phi}$ and $\hat{\boldsymbol{z}}^{\phi}$ is transformed version of $\boldsymbol{z}^{\phi}$ with operator $\mathbf{P}$. For computation without using mapping function, firstly $\mathbf{\Sigma}_1$ is centralized [19] by,

$$\tilde{\mathbf{\Sigma}}_1 = \mathbf{\Sigma}_1 - \mathbf{I}_M\mathbf{\Sigma}_1 - \mathbf{\Sigma}_1\mathbf{I}_M + \mathbf{I}_M\mathbf{\Sigma}_1\mathbf{I}_M \tag{13}$$

where, $\mathbf{I}_{\mathrm{M}}$ is the matrix which has the same elements of $1/\mathrm{M}$. The eigenvectors of $\tilde{\mathbf{\Sigma}}_1$ $(\boldsymbol{\theta}_1, \boldsymbol{\theta}_2, \ldots, \boldsymbol{\theta}_{m_1})$ corresponding to the m_1 largest eigenvalues $\lambda_1 \geq \lambda_2 \geq \ldots \geq \lambda_{m_1}$ are obtained. Then, for the training vectors of class one, the i^{th} feature vector $\mathrm{f_i}$ of the testing vector $\boldsymbol{z}$:

$$f_i = \frac{1}{\sqrt{\lambda_i}}\boldsymbol{\theta}_i{}^{\mathrm{T}}[K(\boldsymbol{a}_1,\boldsymbol{z}), K(\boldsymbol{a}_2,\boldsymbol{z}), \ldots, K(\boldsymbol{a}_M,\boldsymbol{z})]. \tag{14}$$

The feature vector $\boldsymbol{f} = [f_1, f_2, \ldots, f_{m_1}]$ is transformed into $\hat{\boldsymbol{f}} = \mathbf{P}^T\boldsymbol{f}$. Finally, $\hat{\boldsymbol{f}}$ projected onto the subspaces

$$\begin{aligned}\mathbf{R}_1 &= \mathbf{V}_1{}^{\mathrm{T}}\hat{\boldsymbol{f}} \\ \mathbf{R}_2 &= \mathbf{V}_2{}^{\mathrm{T}}\hat{\boldsymbol{f}}\end{aligned} \tag{15}$$

Now, we can rewrite the (12)

$$\mathrm{y}_{\mathrm{out}} = \mathbf{R}_1^{\mathrm{T}}\mathbf{R}_1 - \mathbf{R}_2^{\mathrm{T}}\mathbf{R}_2 \tag{16}$$

Equation (16) can be utilized as a decision rule in KFKT-based QCF design.

III. Experimental Results

In this section, we will show the classification performance of our proposed framework on real HSI. In this experiment, the training spectral vectors, extracted previously on an independent data set, were used as an input of KFKT-based classifier. The sample spectral signatures of meat and fat are given in Fig. 3. Designed classifier tries to segment the fat content of the ground meat by regarding the fat as target class. For representation of class two in KFKT, we utilized training samples of pure meat content.

To construct KFKT from classical FKT, we exploited the RBF kernel which has single free parameter σ. The parameter σ in the RBF kernel should be determined appropriately to achieve a sufficient classification performance. In [20], a Differential Evolution algorithm based kernel parameter selection technique for KFKT has been proposed. In this study, the kernel parameter is determined experimentally. Then, we have employed KFKT to detect percentage of the fat. After obtaining similarity map of fat content via KFKT, a user-defined threshold value is applied to map. Finally, the

whole area of ROI is divided by thresholded pixelwise fat region, so the ratio of fat content is predicted. Table II reports the true percentage of fat content and the fat percentage estimated by KFKT-based technique.

TABLE II
REAL AND ESTIMATED PERCENTAGES OF FAT CONTENT

Data Set	VNIR – 187 bands
Real Percentage	64.29
Our prediction	63.53

From Table II, we can find that the estimation percentage of the employed technique is considerably close to the real value.

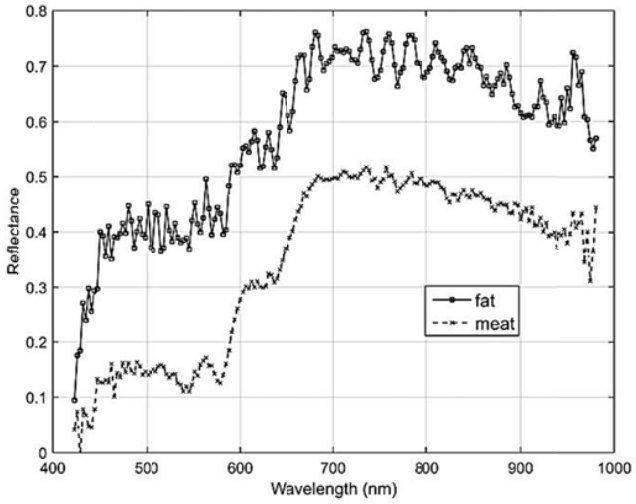

Fig. 3 Sample spectral signatures

IV. CONCLUSION

HSI fuses two attractive technologies, i.e., spectroscopy and computer vision. This phenomenon allows researchers to give both spectral and textural features of food products simultaneously. Such copiousness in information brings a broad platform for employing numerous pattern recognition techniques and multivariate data analyses to expose quality and safety characteristic features in the food materials.

In this paper, we have considered the estimation of fat content of ground meat on hyperspectral images. For this purpose, we have employed KFKT-based classification algorithm. The experimental results show that the proposed supervised framework is effective and suitable for computer vision-based inspection of food products. The main drawback of this technique is to need much computation time just as other kernel-based.

Even though we use KFKT to estimate of fat content of ground meat in this work, apparently it can be employed to solving any problems involving two-patterns in food inspection.

ACKNOWLEDGMENT

The authors would like to thank the YTU-YAZGI Laboratory Team for providing the HSI data.

REFERENCES

[1] A. A. Gowen, C. P. O'Donnell, P. J. Cullen, G.Downey, and J. M. Frias, "Hyperspectral imaging - an emerging process analytical tool for food quality and safety control," *Trends in Food Science &Technology*, vol. 18, pp. 590–598, 2007.
[2] R. W. Basedow, D. C. Carmer, and M. L. Anderson, "HYDICE System, Implementation and Performance," *SPIE Proc.*, vol. 2480, pp. 258-267, Orlando, FL, 17-18 April 1995.
[3] N. Gupta, and R. Dahmani, "Multispectral and hyperspectral imaging with AOTF for object recognition," *The 27th AIPR Workshop: Advances in Computer-Assisted Recognition. International Society for Optics and Photonics*, pp. 128-135, 1999.
[4] D. Manolakis, D. Marden, and G. A. Shaw, "Hyperspectral image processing for automatic target detection applications," *Lincoln Laboratory Journal*, vol. 14, no. 1, pp. 79-116, 2003.
[5] G. P. Petropoulos, C. Kalaitzidis, and K. P. Vadrevu, "Support vector machines and object-based classification for obtaining land-use/cover cartography from Hyperion hyperspectral imagery," *Computers & Geosciences*, vol. 41, pp. 99-107, 2012.
[6] C. Balas, "Review of biomedical optical imaging—a powerful, non-invasive, non-ionizing technology for improving in vivo diagnosis," *Measurement science and technology*, vol. 20, no. 10, 104020, 2009.
[7] Y. Z. Feng, and D. W. Sun, "Application of hyperspectral imaging in food safety inspection and control: a review," *Critical reviews in food science and nutrition*, vol. 52, no. 11, pp. 1039-1058, 2012.
[8] H. Huang, L. Liu, and M. O. Ngadi, "Recent developments in hyperspectral imaging for assessment of food quality and safety," *Sensors*, vol. 14, no. 4, pp. 7248-7276, 2014.
[9] R. Liu, E. Liu, J. Yang, T. Zhang, and F. Wang, "Infrared small target detection with kernel Fukunaga-Koontz transform," *Meas. Sci. Technol*, vol. 18, no. 9, pp. 3025-3035, 2007.
[10] H. Binol, G. Bilgin, S. Dinc, and A. Bal, "Kernel Fukunaga-Koontz Transform Subspaces for Classification of Hyperspectral Images with Small Sample Sizes," *IEEE Geosci. and Rem. Sens. Let.*, vol. 12, no. 6, pp. 1287-1291, 2015.
[11] Y-H. Li, and M. Savvides, "Kernel Fukunaga-Koontz transform subspaces for enhanced face recognition," in *IEEE Conf. on Computer Vision and Pattern Recognition* (CVPR 2007), pp. 1-8, June 2007.
[12] X. Zhang, F. Liu, Y. He, and X. Li, "Application of hyperspectral imaging and chemometric calibrations for variety discrimination of maize seeds," *Sensors,* vol. 12, no. 12, pp. 17234-17246, 2012.
[13] H. Grahn, and P. Geladi, eds. *Techniques and applications of hyperspectral image analysis*. John Wiley & Sons, 2007.
[14] K. Fukunaga and W. L. G. Koontz, "Applications of the Karhunen-Loève expansion to feature selection and ordering," *IEEE Transaction on Computers*, vol.19, no. 5, pp. 311–318, 1970.
[15] S. R. F. Sims, and A. Mahalanobis, "Performance evaluation of quadratic correlation filters for target detection and discrimination in infrared imagery," *Optical Engineering*, vol. 43, pp. 1705 -1711, 2004.
[16] M. Aizerman, E. Braverman, and L. Rozonoer, "Theoretical foundations of the potential function method in pattern recognition learning," *Automation and Remote Control*, vol. 25, pp. 821-837, 1964.
[17] J. Shawe-Taylor, and N. Cristianini, *Kernel Methods for Pattern Analysis.* Cambridge: Cambridge University Press, 2004.
[18] X. Huo, et al., "Optimal Reduced-Rank Quadratic Classifiers using the Fukunaga-Koontz Transform with Applications to Automatic Target Recognition," *Proceedings of SPIE*, vol. 5094, 2003.
[19] J. Yang, A. F. Frangi, J. Y. Yang, D. Zhang, and Z. Jin, Z, "KPCA plus LDA: a complete kernel Fisher discriminant framework for feature extraction and recognition," *Pattern Analysis and Machine Intelligence, IEEE Transactions on*, vol. 27, no. 2, pp. 230-244, 2005.
[20] H. Binol , A. Bal, and H. Cukur, "Differential evolution algorithm-based kernel parameter selection for Fukunaga-Koontz Transform subspaces construction," *Proc. SPIE*, *High-Performance Computing in Remote Sensing V*, vol. 9646, October 2015.